LETTERS
PUBLISHED ONLINE: 6 FEBRUARY 2017 | DOI: 10.1038/NNANO.2016.302
nature nanotechnology

Heat transport through atomic contacts

Nico Mosso*, Ute Drechsler, Fabian Menges, Peter Nirmalraj, Siegfried Karg, Heike Riel and Bernd Gotsmann*

Heat transport and dissipation at the nanoscale severely limit the scaling of high-performance electronic devices and circuits[1]. Metallic atomic junctions serve as model systems to probe electrical and thermal transport down to the atomic level as well as quantum effects that occur in one-dimensional (1D) systems[2]. Whereas charge transport in atomic junctions has been studied intensively in the past two decades[2–5], heat transport remains poorly characterized because it requires the combination of a high sensitivity to small heat fluxes and the formation of stable atomic contacts. Here we report heat-transfer measurements through atomic junctions and analyse the thermal conductance of single-atom gold contacts at room temperature. Simultaneous measurements of charge and heat transport reveal the proportionality of electrical and thermal conductance, quantized with the respective conductance quanta[6]. This constitutes a verification of the Wiedemann–Franz law at the atomic scale[7].

The development of experimental techniques, such as scanning tunnelling microscopy (STM) and mechanically controlled break junction enabled the formation and manipulation of monoatomic metallic chains[3–5]. Using similar techniques, Joule dissipation[8,9] and thermoelectric effects[10,11] have been probed recently. Nonetheless, the properties of heat conduction through atomic junctions remain to be explored fully.

Electrical conductance in atomic junctions is quantized. A single gold atom contact has a conductance equal to the quantum $G_0 = 2e^2/h$, where e is the electron charge and h is Planck's constant. The Landauer approach used to describe charge transport can also be applied to heat transport[12] and it predicts the validity of the Wiedemann–Franz law. This states that the thermal conductance G_{th} and the electrical conductance G_{el} are proportional to each other:

$$G_{\text{th}} = L_0 T G_{\text{el}} \tag{1}$$

where T is the absolute temperature and the proportionality factor L_0, called the Lorenz number, assumes the universal Sommerfeld value, $L_0 = 2.44 \times 10^{-8}\ \text{V}^2\ \text{K}^{-2}$. The Wiedemann–Franz law applies to systems in which heat is predominantly transported by electrons and holds to a good approximation when scattering is mostly elastic[13]. This is largely valid for bulk metals at high and low temperature and is also expected for metallic point contacts. Verification of the Wiedemann–Franz law for metallic nanostructures, however, has proved to be difficult. Both enhancements[14–16] and reductions[17,18] of the Lorenz number have been reported, which debates its general validity.

Marked deviations from the Wiedemann–Franz law can occur when electrons are physically confined in 1D systems in which the Fermi liquid state is replaced by a Tomonaga–Luttinger liquid state[19], as experimentally demonstrated for isolated monoatomic gold chains[20]. Owing to the 1D confinement of electrons, spin-charge separation occurs and enables scattering mechanisms to affect charge and heat transport independently. Although atomic junctions are well described by the Fermi liquid theory, no experimental demonstration on the validity of the Wiedemann–Franz law at this scale has been reported so far. To date, most heat-transport measurements in metallic ballistic systems come from 1D channels defined in 2D electron gases at low temperature[21,22].

Investigation of the heat-conduction properties at the atomic scale, however, poses difficult experimental challenges in terms of thermal sensitivity and mechanical stability. Here we circumvent these challenges by using a micro electromechanical system (MEMS) with an integrated thermal sensor that is operated within a vacuum-based scanning tunnelling microscope (STM) inside the IBM's Noise Free Labs[23]. The experimental technique is schematically represented in Fig. 1. The system essentially combines simultaneous measurements of heat and charge transport to extract the thermal and electrical conductance of metallic contacts. Similar to other STM break-junction set-ups[24], an STM tip is used to form and break few-atom contacts on a substrate covered by a metallic layer. Here, however, the bottom electrode is integrated on a suspended MEMS to insulate it thermally from the chip substrate. The membrane also features a platinum microheater that is used to control and monitor its temperature via Joule dissipation and a four-point measurement of the heater electrical resistance, respectively. (Supplementary Information, page 4).

The measurements are performed under high-vacuum conditions at room temperature, T_{amb}. During the measurement, the membrane is heated to a certain temperature T_{H} through Joule dissipation into the heater with the STM tip kept at room temperature (T_{amb}). Using a piezoelectric element, the STM tip is then approached towards the hot electrode until an electrical contact forms. By measuring the induced temperature change in the MEMS, the thermal conductance G_{Au} of the contact can be extracted. The tip is then retracted until the contact is broken. During the breaking process, the contact size can be reduced to a single atom[3], as verified by the simultaneous measurement of the electrical conductance quantum G_0. This formation and breaking process is then repeated several thousands of times to obtain statistically relevant information about the quantum point contact properties.

The total thermal conductance can be calculated according to equation (2):

$$G_{\text{tot}} = \frac{\dot{Q}_{\text{tot}}}{\Delta T} \tag{2}$$

with $\dot{Q}_{\text{tot}}$ representing the total heat flux provided to the membrane, which induces a temperature change, $\Delta T = (T_{\text{H}} - T_{\text{amb}})$.

Prior to contact formation (Fig. 1c), the total heat provided, $\dot{Q}_{\text{tot}}$, is equal to the effective power dissipated, P_{H}, in the heater and the metallic lines and the total thermal conductance, $G_{\text{tot}} = G_{\text{MEMS}}$, corresponds to the contribution to heat conduction of the

IBM Research – Zurich, Säumerstrasse 4, 8803 Rüschlikon, Switzerland. *e-mail: bgo@zurich.ibm.com; nmo@zurich.ibm.com

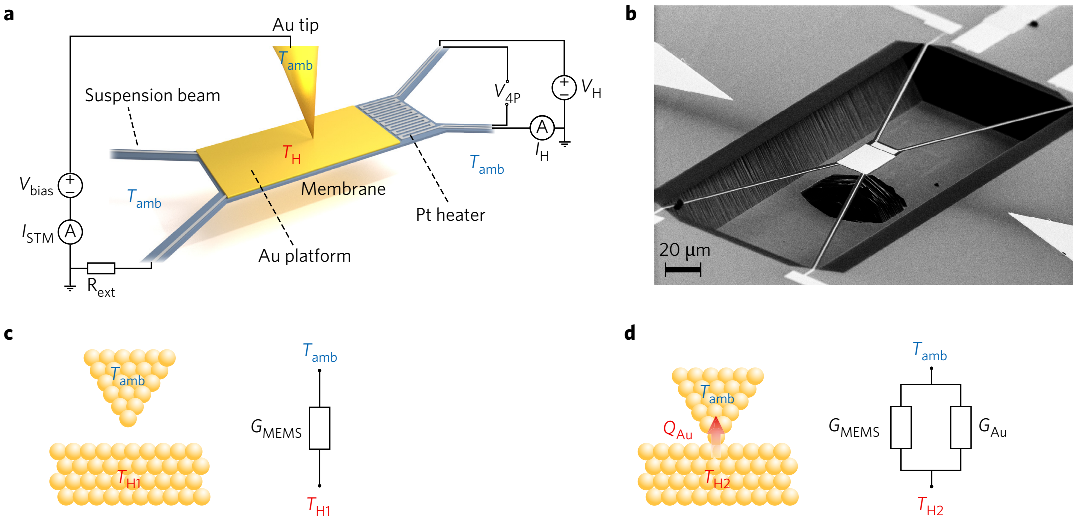

Figure 1 | Schematic representation of the measurement technique. **a**, Schematic diagram of the experiment. To monitor the temperature, T_H, of the gold electrode, the four-probe (4P) voltage, V_{4P}, and the heater current, I_H, are measured. Simultaneous measurement of the tunnelling current, I_{STM}, allows us to extract the electrical resistance of the junction. An external resistor R_{ext} limits the current. **b**, Scanning electron micrograph of the MEMS used in this work. The MEMS consists of a silicon nitride membrane 150 nm thick with four 3.5 µm wide and 255 µm long suspension beams (Supplementary Information, page 2). **c**, Prior to contact formation, the membrane is heated to T_{H1}. The total thermal conductance of the system is given only by the contribution of the suspension beams of the MEMS. **d**, After contact formation, the temperature of the membrane decreases to T_{H2}, with $T_{H2} < T_{H1}$. The total thermal conductance is now given by the sum of the thermal conductance of the MEMS (G_{MEMS}) and that of the quantum point contact (G_{Au}).

suspension beams. Once the contact has formed, the thermal conductance increases, $G_{tot} = G_{MEMS} + G_{Au}$, as shown in Fig. 1d. By subtracting the in- and out-of-contact values we obtain the thermal conductance of the gold–gold contact, G_{Au}. In calculating the total heat provided to the membrane, $\dot{Q}_{tot}$, the power dissipated in the STM circuit, P_{STM}, must be accounted for, $\dot{Q}_{tot} = P_H + P_{STM}$.

Clearly, the thermal conductance of the MEMS plays a crucial role in determining the sensitivity of the measurement. Indeed, G_{MEMS} must be designed to be as close as possible to G_{Au} so that there is sufficient contrast in the thermal conductance when only a few atoms connect the tip to the membrane. However, to reduce G_{MEMS} also means that the mechanical stiffness of the MEMS is decreased. The device used for this experiment features a thermal conductance, $G_{MEMS} = 3.4 \times 10^{-8}$ W K^{-1}, with an estimated vertical stiffness lower than the stiffness of a single Au–Au contact and is therefore not suitable *a priori* to achieve a controlled breaking process. In fact, with a purely vertical motion of the tip, we observed an abrupt breaking from large contacts ($G_{el} > 10\ G_0$) to tunnelling in most of the traces. For this reason, the tip was approached and retracted at an angle of about 25° with respect to the in-plane direction of the membrane. Thus, by taking advantage of the larger in-plane stiffness of the MEMS, it was possible to break the metallic contact within a displacement of the tip of a few nanometres. Also, the gold surface exhibits some significant roughness on the order of nanometres (unlike the idealized schematic in Fig. 1), which is expected to influence the breaking process (Supplementary Information, from page 2).

Figure 2 shows an example of an opening trace of a gold–gold junction, measured at a fixed $V_{bias} = 50$ mV. In Fig. 2a, we observe that the initial gold–gold contact is made of a few atoms that feature an electrical conductance of about 6 G_0. When retracting the tip, the gold contact shrinks and the electrical conductance decreases in a typical step-like fashion that is characteristic of the 1D ballistic transport regime. In particular, the plateau at around 1 G_0 indicates the formation of a single-atom contact. After breaking the contact (at about 4.5 nm), we enter the tunnelling regime. In Fig. 2b, the thermal conductance follows the trend of the electrical conductance trace, albeit with a characteristic delay given by the thermal time constant of the MEMS of $\tau = 30$ ms, as measured from the step response of the heater during calibration.

In Fig. 3 we show the 2D histogram that correlates the thermal with the charge-transport data. The axes are plotted as multiples of the electrical and thermal conductance quanta, respectively G_0 and $G_Q = L_0 T G_0$, where L_0 is the Lorenz number and $T = (T_H + T_{amb})/2$ is the average contact temperature. From this graph, we can clearly deduce that the thermal and electrical conductances are proportional to each other in such few-atom contacts, independent of the contact size. The 2D histogram was built by selecting ~2,000 traces that fell in the temperature range $\Delta T = 35$–50 K between the tip and the membrane. During the measurement, reconfiguration of the tip and membrane surface can lead to thermal short cutting of the MEMS and thereby loss of sensitivity, owing to molecular contamination or parasitic coupling of near-field radiation. To verify that the correlation between the thermal and the electrical transport signals is not affected by effects other than those considered, we repeated the measurements using different voltage-bias values and sign up to $V_{bias} = 300$ mV. Under such high bias conditions, the contribution of the electronic dissipation at the junction and in the supporting beam cannot be neglected, as we observed a net increase of temperature in the platform instead of a net cooling through the atomic contact. The results (Supplementary Fig. 5) confirm our interpretation, and the underlying assumption that heat dissipation in atomic-scale gold contacts occurs symmetrically in the electrodes, as shown recently[8]. The temperature difference across the contact varied within certain limits because of the aforementioned Joule dissipation effects and parasitic conductance effects. The temperature difference range available to us was limited to a maximum of ~50 K (to avoid buckling and mechanical instabilities of the MEMS platform). In all cases the normalization of the heat current by temperature difference led to consistent values of thermal conductance.

In Fig. 4, we plot the thermal versus the electrical conductance extracted from the median of the 2D histogram. Experimental uncertainties and systematic errors are included, which take into account the offsets of the analogue–digital and digital–analogue converters, the amplifier gains, Seebeck voltages and the temperature

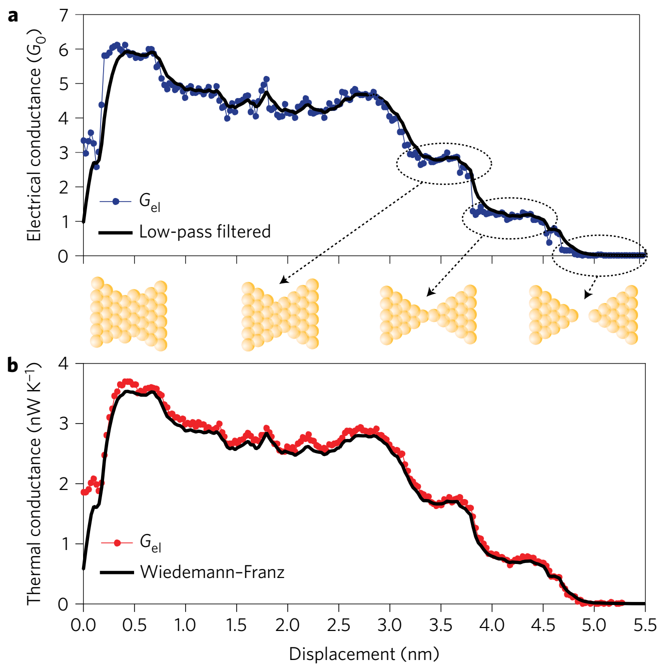

Figure 2 | Thermal and electrical conductance of a gold-gold contact during the breaking process. a,**b**, Both the thermal and the electrical conductance show quantization steps at multiples of G_0, in agreement with the Wiedemann–Franz law. The black line in **a** was calculated by digitally low-pass filtering the electrical conductance G_{el} with the thermal time constant value $\tau = 30$ ms from calibration. The black line in **b** was calculated by applying the Wiedemann–Franz law to the aforementioned low-pass filtered signal. The sampling time was set to 10 ms and the tip was retracted with an angle of about 25° with respect to the gold surface and a speed of ~3 nm s^{-1}. The x axis corresponds to the displacement of the tip versus the gold surface. The bias voltage applied was 50 mV, corresponding to ~5 mV at the single-atom contact owing to the series resistance (Supplementary Information, page 7). ΔT ranges from 41.5 K to 43.6 K, from closed (6 G_0) to open contact, respectively. Further examples of single traces are provided in Supplementary Fig. 3.

dependence of the series resistance (Supplementary Information). The measured thermal conductance comprises the contribution of all the heat carriers, including electrons, phonons and radiation: $G_{Au} = G_{electrons} + G_{phonons} + G_{radiation}$. The contribution of radiation between two metals[25,26] is weak, but may still reach magnitudes similar to our signal depending on the exact local geometry of the tip and surface around the junction. For blunter tips or owing to spurious contaminants, we observe a distance dependence of the thermal signal in the non-contact region (for example, in Fig. 2 for displacements greater than 5 nm). However, by using electrochemically etched Au tips, we were able to collect data in which these effects appear only as a constant offset or are negligible. The phonon contribution to thermal conductance can be estimated from existing models for both single-atom contacts and larger ballistic contacts, albeit with significant uncertainty. The scaling with contact size should follow approximately the scaling of electrical conductance in a situation in which both charge and phonon transport are in the ballistic regime. We estimate the phonon contribution to be between the bounds 2 and 22% of the Wiedemann–Franz law (Supplementary Information, page 12).

Comparing now the theoretical prediction with our experimental data (Fig. 4), we find quantitative agreement within the respective uncertainties. Although the experimental sensitivity, in principle, falls within the range of the expected phonon contribution, the overall uncertainty of the total G_{Au} does not allow an assessment of the possible limits of phonon transport. However, we do not observe a significant difference in the measured Lorenz number and the Sommerfeld value L_0. Interestingly, these findings appear to be robust against variations in the contact details. For example, tunnelling through small molecules may still recover the Wiedemann–Franz signature. Both the electrical and thermal conductance 1D histograms in Fig. 3 show single-atom peaks with mean positions shifted to higher values (~1.3 G_0 and ~1.3 G_Q, respectively) and sharp peaks around ~0.4 G_0 and ~0.4 G_Q,

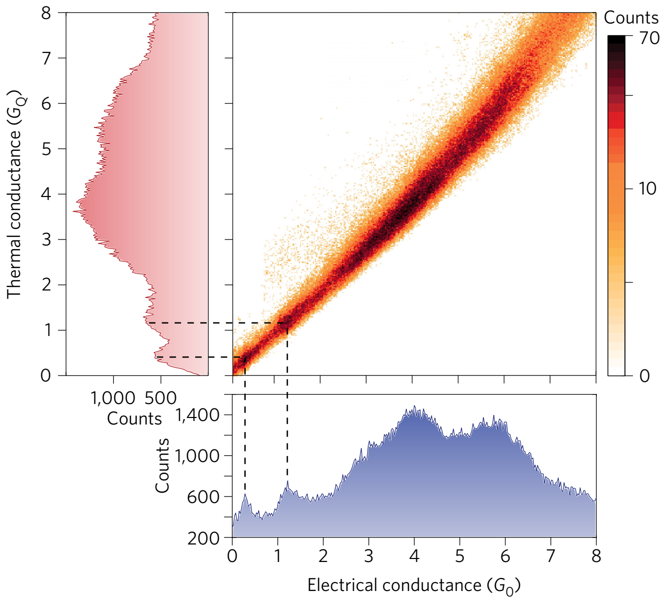

Figure 3 | 2D histogram of thermal versus electrical conductance with respective projections onto 1D histograms. The 2D histogram shows that the linear proportionality between the thermal and electrical conductance holds at different contact sizes. The histogram was built from about 2,000 out of 5,000 traces selected in the temperature range $\Delta T = 35$–50 K between the tip and membrane (Supplementary Fig. 4). The thermal conductance was normalized by the thermal conductance quantum G_Q. The thermal and electrical 1D histograms were built with a linear binning and a bin size of 0.025 G_Q and 0.025 G_0, respectively.

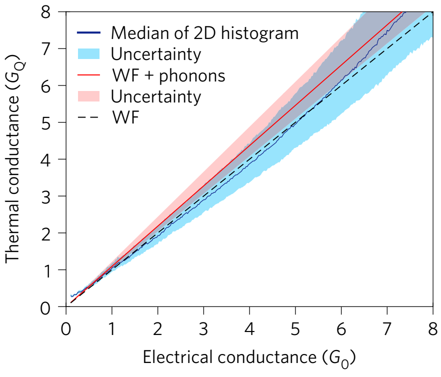

Figure 4 | Comparison between the experimental findings and the theoretical prediction. The median of the 2D histogram shown in Fig. 3 is reported in comparison with the estimated thermal conductance of the quantum point contact. The dashed black line represents the electron contribution as predicted by the Wiedemann–Franz (WF) law. The red continuous line also takes into account the phonon contribution to heat transport through the quantum point contact. The shaded areas represent the uncertainty regions (Supplementary Information, page 7).

respectively. According to the literature, the absorption of CO molecules on gold electrodes introduces an additional peak at 0.2–0.3 G_0 (refs 27,28) or at 0.7 G_0 (refs 28,29) and may induce a shift of the G_0 peak[27]. In our case, we can expect CO molecules to be present on the Au surface even after wet chemical and heat cleaning. As an important cross-check, we find that the position of the single-atom peak is related to the intensity of the peak at ~0.4 G_0 (Supplementary Fig. 6). However, other common small-molecule species, such as H_2O, have been related to similar sub-G_0 conductance features. Therefore, further studies are needed to corroborate this preliminary conclusion.

In summary, we have measured the thermal conductance of metallic quantum point contacts down to the single-atom level at room temperature. The experimental results confirm the validity of the Wiedemann–Franz law in quantum point contacts as predicted by the Landauer approach for heat transport. To achieve these results, we developed an experimental technique that allows the simultaneous measurement of heat and charge transport in atomic contacts. By further improving such techniques it may also be possible to investigate phonon transport in contacts at the single-atom scale, which may be used to verify conclusions drawn from previous studies of the mechanical contacts of atomically rough surfaces[30]. This will enable heat transport to be investigated not only in quantum point contacts of different metals, but also in molecular junctions, a fundamental scientific and technological step forwards in managing and controlling heat at the nanoscale.

Data availability statement. The data that support the plots within this paper and other findings of this study are available from the corresponding authors on reasonable request. Source data for all the figures provided within the paper are in the Supplementary Information.

Received 29 June 2016; accepted 28 December 2016;
published online 6 February 2017

References

1. Pop, E. Energy dissipation and transport in nanoscale devices. *Nano Res.* **3,** 147–169 (2010).
2. Agraït, N., Yeyati, A. L. & van Ruitenbeek, J. M. Quantum properties of atomic-sized conductors. *Phys. Rep.* **377,** 81–279 (2003).
3. Yanson, A. I., Bollinger, G. R., van den Brom, H. E., Agraït, N. & van Ruitenbeek, J. M. Formation and manipulation of a metallic wire of single gold atoms. *Nature* **395,** 783–785 (1998).
4. Muller, C. J., Krans, J. M., Todorov, T. N. & Reed, M. A. Quantization effects in the conductance of metallic contacts at room temperature. *Phys. Rev. B* **53,** 1022–1025 (1996).
5. Ohnishi, H., Kondo, Y. & Takayanagi, K. Quantized conductance through individual rows of suspended gold atoms. *Nature* **395,** 780–783 (1998).
6. Schwab, K., Henriksen, E. A., Worlock, J. M. & Roukes, M. L. Measurement of the quantum of thermal conductance. *Nature* **404,** 974–977 (2000).
7. Franz, R. & Wiedemann, G. Ueber die Wärme-Leitungsfähigkeit der metalle. *Ann. Phys.* **165,** 497–531 (1853).
8. Lee, W. *et al.* Heat dissipation in atomic-scale junctions. *Nature* **498,** 209–212 (2013).
9. Tsutsui, M., Kawai, T. & Taniguchi, M. Unsymmetrical hot electron heating in quasi-ballistic nanocontacts. *Sci. Rep.* **2,** 217 (2012).
10. Evangeli, C. *et al.* Quantum thermopower of metallic atomic-size contacts at room temperature. *Nano Lett.* **15,** 1006–1011 (2015).
11. Tsutsui, M., Morikawa, T., Arima, A. & Taniguchi, M. Thermoelectricity in atom-sized junctions at room temperatures. *Sci. Rep.* **3,** 3326 (2013).
12. Butcher, P. N. Thermal and electrical transport formalism for electronic microstructures with many terminals. *J. Phys. Condens. Matter* **2,** 4869–4878 (1990).
13. Ashcroft, N. W. & Mermin, N. *Solid State Physics* (Saunders College, 1976).
14. Zhang, Q. G., Cao, B. Y., Zhang, X., Fujii, M. & Takahashi, K. Influence of grain boundary scattering on the electrical and thermal conductivities of polycrystalline gold nanofilms. *Phys. Rev. B* **74,** 134109 (2006).
15. Ou, M. N., Yang, T. J., Harutyunyan, S. R., Chen, Y. Y. & Chen, C. D. Electrical and thermal transport in single nickel nanowire. *Appl. Phys. Lett.* **92,** 063101 (2008).
16. Cheng, Z., Liu, L., Xu, S., Lu, M. & Wang, X. Temperature dependence of electrical and thermal conduction in single silver nanowire. *Sci. Rep.* **5,** 10718 (2015).
17. Völklein, F., Reith, H., Cornelius, T. W., Rauber, M. & Neumann, R. The experimental investigation of thermal conductivity and the Wiedemann–Franz law for single metallic nanowires. *Nanotechnology* **20,** 325706 (2009).
18. Avery, A. D., Mason, S. J., Bassett, D., Wesenberg, D. & Zink, B. L. Thermal and electrical conductivity of approximately 100-nm permalloy, Ni, Co, Al, and Cu films and examination of the Wiedemann–Franz Law. *Phys. Rev. B* **92,** 1–10 (2015).
19. Wakeham, N. *et al.* Gross violation of the Wiedemann–Franz law in a quasi-one-dimensional conductor. *Nat. Commun.* **2,** 396 (2011).
20. Blumenstein, C. *et al.* Atomically controlled quantum chains hosting a Tomonaga–Luttinger liquid. *Nat. Phys.* **7,** 776–780 (2011).
21. Chiatti, O. *et al.* Quantum thermal conductance of electrons in a one-dimensional wire. *Phys. Rev. Lett.* **97,** 1314 (2006).
22. Molenkamp, L. W., Gravier, T., van Houten, H., Buijk, O. J. A. & Mabesoone, M. A. A. Peltier coefficient and thermal conductance of a quantum point contact. *Phys. Rev. Lett.* **68,** 3765–3768 (1992).
23. Lörtscher, E., Widmer, D. & Gotsmann, B. Next-generation nanotechnology laboratories with simultaneous reduction of all relevant disturbances. *Nanoscale* **5,** 10542 (2013).
24. Pascual, J. I. *et al.* Quantum contact in gold nanostructures by scanning tunneling microscopy. *Phys. Rev. Lett.* **71,** 1852–1855 (1993).
25. Kim, K. *et al.* Radiative heat transfer in the extreme near field. *Nature* **528,** 387–391 (2015).
26. Kittel, A. *et al.* Near-field heat transfer in a scanning thermal microscope. *Phys. Rev. Lett.* **95,** 1–4 (2005).
27. Den Boer, D. *et al.* Electron transport through CO studied by gold break-junctions in nonpolar liquids. *J. Phys. Chem. C* **113,** 15412–15416 (2009).
28. Balogh, Z., Makk, P. & Halbritter, A. Alternative types of molecule-decorated atomic chains in Au–CO–Au single-molecule junctions. *Beilstein J. Nanotechnol.* **6,** 1369–1376 (2015).
29. Kiguchi, M., Djukic, D. & van Ruitenbeek, J. M. The effect of bonding of a CO molecule on the conductance of atomic metal wires. *Nanotechnology* **18,** 35205 (2007).
30. Gotsmann, B. & Lantz, M. A. Quantized thermal transport across contacts of rough surfaces. *Nat. Mater.* **12,** 59–65 (2012).

Acknowledgements

We acknowledge funding by the European Commission FP7 ITN 'MOLESCO' Project No. 606728. We thank J. Repp, K. Moselund and W. Riess for management support of the project. We acknowledge technical support from M. Tschudy, H. Wolf, E. Lörtscher, S. Reidt, A. Olziersky, G. Meyer and C. Bolliger. We thank C. Lambert, H. Sadeghi, G. Signorello, F. Motzfeld, J. Gooth and all the MOLESCO partners for fruitful discussions concerning this work. This work is dedicated to the MOLESCO partner T. Wandlowski.

Author contributions

B.G. and N.M. conceived the experiment. N.M. performed the measurements with the help of P.N., S.K., F.M. and B.G. The MEMS devices were fabricated by U.D. The experiment was designed by B.G., N.M. and F.M. N.M. and B.G. performed the data analysis and wrote the manuscript with contributions by all the authors. All the authors discussed the results.

Additional information

Supplementary information is available in the online version of the paper. Reprints and permissions information is available online at www.nature.com/reprints. Correspondence and requests for materials should be addressed to N.M. and B.G.

Competing financial interests

The authors declare no competing financial interests.